Journal of Nanobiotechnology

RESEARCH Open Access

Smart photonic crystal hydrogels for visual glucose monitoring in diabetic wound healing

Xuxia Yang[1], Langjie Chai[2], Zhuo Huang[2], Bo Zhu[1], Haiyang Liu[1], Zhantian Shi[1], You Wu[1], Liang Guo[2], Longjian Xue[1] and Yifeng Lei[1,3*]

Abstract

Diabetes is a global chronic disease that seriously endangers human health and characterized by abnormally high blood glucose levels in the body. Diabetic wounds are common complications which associate with impaired healing process. Biomarkers monitoring of diabetic wounds is of great importance in the diabetes management. However, actual monitoring of biomarkers still largely relies on the complex process and additional sophisticated analytical instruments. In this work, we prepared hydrogels composed of different modules, which were designed to monitor different physiological indicators in diabetic wounds, including glucose levels, pH, and temperature. Glucose monitoring was achieved based on the combination of photonic crystal (PC) structure and glucose-responsive hydrogels. The obtained photonic crystal hydrogels (PCHs) allowed visual monitoring of glucose levels in physiological ranges by readout of intuitive structural color changes of PCHs during glucose-induced swelling and shrinkage. Interestingly, the glucose response of double network PCHs was completed in 15 min, which was twice as fast as single network PCHs, due to the higher volume fraction of glucose-responsive motifs. Moreover, pH sensing was achieved by incorporation of acid-base indicator dyes into hydrogels; and temperature monitoring was obtained by integration of thermochromic powders in hydrogels. These hydrogel modules effectively monitored the physiological levels and dynamic changes of three physiological biomarkers, both in vitro and in vivo during diabetic wound healing process. The multifunctional hydrogels with visual monitoring of biomarkers have great potential in wound-related monitoring and treatment.

Introduction

Diabetes is a global chronic disease characterized by abnormally high blood glucose levels and poses a serious threat to human health [1]. With the change of human lifestyle and the aging of population, the number of people with diabetes mellitus continues to rise worldwide. Among the various complications, diabetic wound is one of the most common complications [2]. Different from normal wound healing process, diabetic patients suffered from impaired wound healing [3], due to a complex wound microenvironment associated with high blood glucose levels, high levels of inflammatory cytokines, and excessive exudate, which making the diabetic wounds difficult to enter the proliferation and remodeling phases, thus hindering the healing process of diabetic wounds.

Different wound microenvironments, such as glucose levels, pH value, ROS level, temperature, humidity and wound pressure, could affect or reflect the diabetic wound healing process [2, 4]. Real-time monitoring of diabetic wound-related biomarkers is important for the timely assessment of the condition and the stage of wound development [5]. Conversely, real-time evaluation of the efficacy of wound healing is essential for effective

*Correspondence:
Yifeng Lei
yifenglei@whu.edu.cn

Full list of author information is available at the end of the article

Graphical abstract

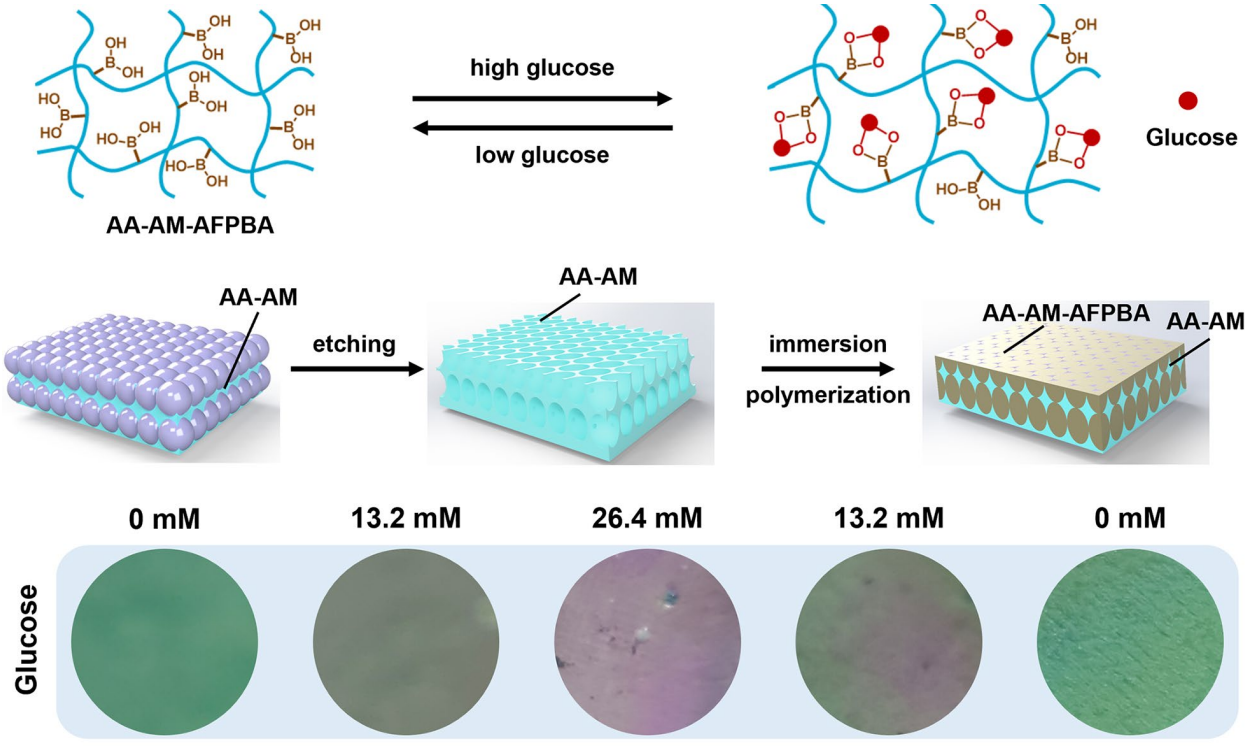

Keywords Diabetic wounds, Glucose-responsive hydrogel, Visual monitoring, Photonic crystal, Structure colors

clinical interventions, replace of dressings and optimizing diabetic wound treatment [5]. Ideally, if there exists a smart dressing that can diagnose the diabetic wound healing stage and indicate the right time to change the dressing in the absence of a nursing professional, it would effectively simplify daily care, and reduce the financial burden of diabetes management.

With the development of multifunctional hydrogels and flexible electronics, researchers have developed abundant smart biosensors for monitoring and diagnosis of diabetic wounds microenvironment or revealing the healing status [5, 6], including the biochemical markers such as glucose [7–9], pH [10–13], H_2O_2 [14], lactate [15], mRNA levels [16], as well as physical indicators such as temperature [9] and strain [9], and so on. Typically, optical biosensors of diabetes wounds were developed based on swelling and shrinkage of stimuli-responsive hydrogels [17], using the detection mechanisms of such as wavelength shift [18], change in diffraction pattern [19], change in refractive index [20], variation in diffused light pattern [21], alteration in signal intensity [22], change in surface plasmon resonance (SPR) [23], and so on. The readout mechanisms such as fluorescence [8, 10, 11, 14, 24], spectrometry [25], and colorimetric changes [7, 17, 26, 27] were generally used for analysis. However, these detection approaches still rely on complex process and additional analytical instruments, which are usually expensive and inconvenient to be portable. In practice, more convenient and more direct approach is desired for the real-time monitoring of biomarkers. If visual monitoring of biomarkers by the naked eye could be achieved, it would be easier and quicker to analyze the level of wound indicators, which would be more beneficial in diabetes management.

To this end, visual colors can be integrated into functional hydrogels, offering an emerging strategy to obtain the responsive signals with intuitive color changes. Photonic crystals (PCs) are a class of novel optical structure [28, 29], the structural colors of PCs come from the spatially organized internal periodic microstructure [30, 31], which commonly exist on the body surface of a variety of natural organism such as butterfly and chameleon skins [31]. When the periods of PCs are in the range of a few hundreds of nanometers, the modulation of the incident lights occurs and results in a strengthening in the visible light with the specific wavelength according to Bragg Eqs. [28, 29]. PCs with structural colors have attracted emerging attention in the research field of biosensing [32, 33].

For instance, PCs were integrated on microneedle array for visual monitoring of pH [34, 35] and glucose [35, 36] in interstitial fluid.

Theoretically, system containing glucose-responsive hydrogels can be combined with PCs, to obtain a structural color-based sensing system for naked-eye visualization of the analytes [32, 37, 38]. Herein, we developed a functional hydrogel system for the in-situ monitoring of multiple biomarkers in diabetic wounds, including glucose levels, pH and temperature. To this aim, visual monitoring of glucose was achieved by combination of glucose-responsive hydrogels with the advantages of structure colors of PCs (Fig. 1). The glucose-sensing molecule used in the hydrogel system was (4-((2-acrylamidoethyl)carbamoyl)-3-fluorophenyl)boronic acid (AFPBA) [38–40], which competitively bound to glucose, resulting in the swelling of hydrogels (Fig. 1b). Both single network and double network photonic crystal hydrogels (PCHs) were prepared and investigated for real-time visual glucose monitoring (Fig. 1c-d). Moreover, the pH detection module was accomplished by integration of acid-base indicator into the hydrogels, and the temperature responsive module was developed by incorporation of temperature-responsive thermochromic powders into the hydrogels. We demonstrated the positive response of these functional hydrogels both in vitro in solutions within physiological ranges and in vivo in diabetic wound model in mice. This hydrogel system with visual monitoring of biomarkers has great potential in wound monitoring and managements.

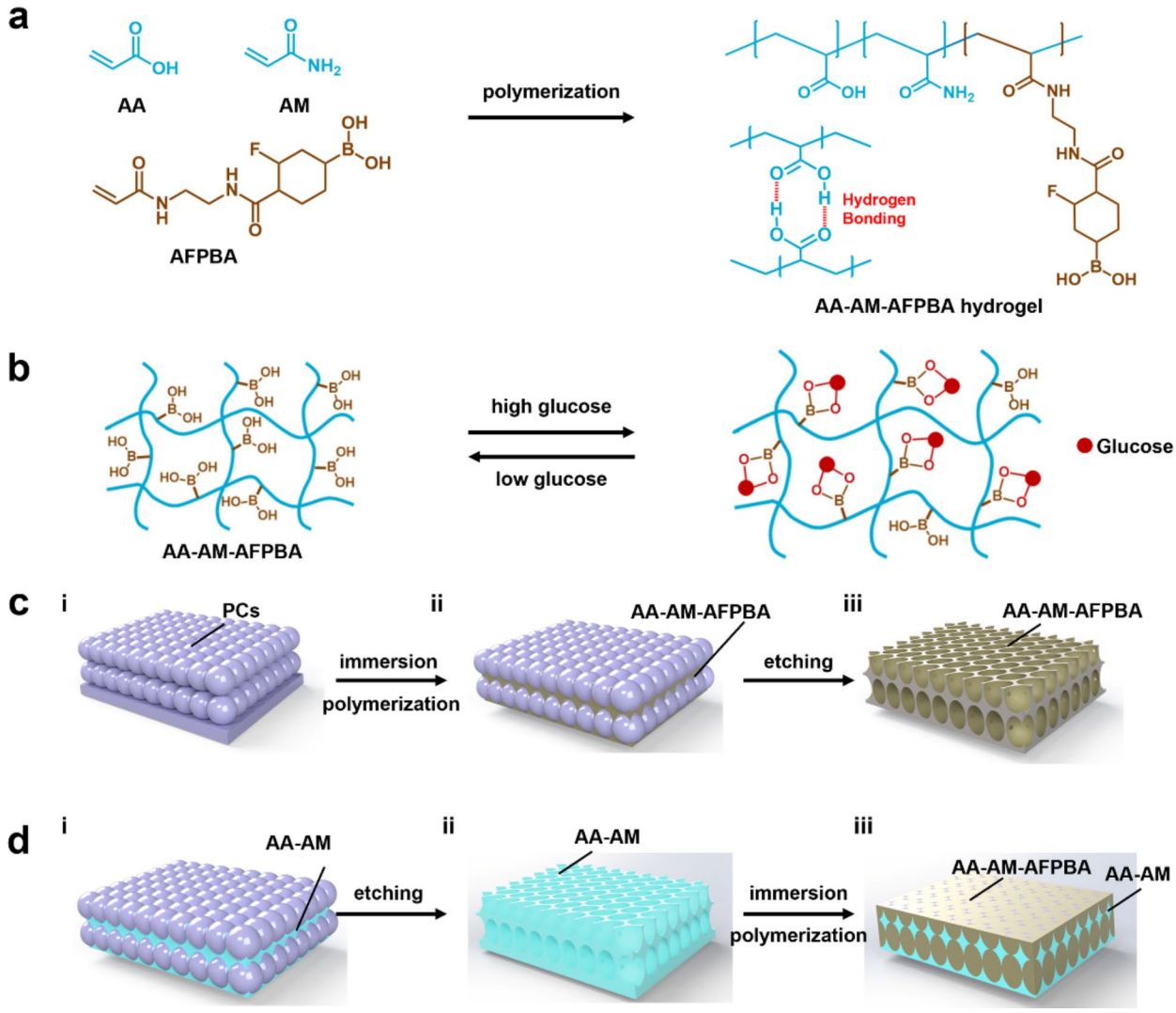

Fig. 1 Schematic illustration of the synthesis and glucose response mechanism of photonic crystal hydrogels (PCHs). (**a**) Illustration of synthesis of AA-AM-AFPBA hydrogel. (**b**) Glucose response mechanism of AA-AM-AFPBA hydrogels. (**c**) Preparation process of single network PCHs consisted of AA-AM-AFPBA hydrogels. (**d**) Preparation process of double network PCHs consisted of AA-AM and AA-AM-AFPBA hydrogels

Experimental section

Materials

Ammonia, ethanol, potassium peroxydisulfate (KPS), phenol red (PR), bromophenol blue (BB), sodium hydroxide, hydrogen peroxide were purchased from Sinopharm, China. Tetraethyl orthosilicate (TEOS), acrylic acid (AA), acrylamide (AM), hydrofluoric acid (HF), D-(+)-glucose, 2-hydroxy-2-methylpropiophenone (PI-1173) were obtained from Aladdin Chemical Co., Ltd. China. N, N'-methylenebisacrylamide (MBAA) was purchased from Shanghai Macklin Biochemical Technology Co., Ltd. (4-((2-acrylamidoethyl)carbamoyl)-3-fluorophenyl)boronic acid (AFPBA) were obtained from Shanghai Bide Pharmaceutical Technology Co., Ltd. Aqueous dispersion of carbon nanotubes (CNTs, 10 mg/mL) was obtained from Shanghai Muke Nanotechnology Co., Ltd. PDMS kits (Sylgard 184) were obtained from Dow Corning, USA. Phosphate buffered saline (PBS, pH 7.4) was obtained from Beijing Solarbio Science & Technology Co., Ltd. Deionized water with a resistivity of 18.2 MΩ.cm (Millipore) was used throughout the experiments.

Preparation of photonic crystals (PCs)

First, SiO_2 nanoparticles with different particle sizes were synthesized according to our previous report [41]. Then, PCs of silica nanoparticles was fabricated with an improved horizontal deposition method [41]. In brief, an enclosure of PDMS (10:1 mass ratio of monomer to curing agent) was prepared on top of a glass slide, with an empty space of 2 mm in depth and 1 cm in diameter. Subsequently, aqueous dispersion of 0.5% (w/v) silica nanoparticles were added dropwise into the PDMS enclosure. Then, the device was heated at 37 °C for evaporation of water, during which the silica nanoparticles were self-assembled on the glass slide, to obtain PCs consisted of silica nanoparticles. Different colors of PCs can be obtained by regulating the particle size of silica nanoparticles from 240 to 320 nm.

Preparation of single network PCHs

Glucose-responsive prepolymer solution was prepared by dissolving 20% (v/v) AA, 10% (w/v) AM, 1% (w/v) AFPBA, 5‰ (w/v) KPS, 3‰ (w/v) MBAA and 2‰ (w/v) CNTs in deionized water. The prepolymer solution of AA-AM-AFPBA hydrogel was added dropwise into the interstices of the above obtained PCs, and heated at 60 °C for 1 h for polymerization (Fig. 1c_{i-ii}). After curing, the sample was immersed in 10% (v/v) HF for 24 h to etch the silica nanoparticles, to obtain the inverse opal structure composed of AA-AM-AFPBA hydrogels (Fig. 1c_{iii}), and was labelled as single network PCHs.

Preparation of double network PCHs

First, inverse opal structure of AA-AM was prepared similarly as above. Briefly, the prepolymer solution of AA-AM hydrogel, which included 20% (v/v) AA, 10% (w/v) AM, 5‰ (w/v) KPS, 3‰ (w/v) MBAA, and 2‰ (w/v) CNTs in deionized water, was injected into the gap of PCs (Fig. 1d_i), cured at 60 °C for 1 h, and etched with HF to obtain the inverse opal structure of AA-AM hydrogels (Fig. 1d_{ii}). Further, the resulting AA-AM inverse opal hydrogel was immersed in the second hydrogel prepolymer solution, which included 20% (v/v) AA, 10% (w/v) AM, 1% (w/v) AFPBA, 2% (v/v) PI-1173, 3‰ (w/v) MBAA. After fulfill in the voids of the inverse opal structure for 5 min, the samples were then fixed between slides and cured by UV light (wavelength 365 nm) irradiation at 80% light intensity (82.10 mW/cm^2) for 3 min. The obtained structure consisted of AA-AM hydrogels as the first network and AA-AM-AFPBA hydrogels as the second network, and was named as double network PCHs (Fig. 1d_{iii}).

Characterization

The microscopic structure of the PCs and PCHs was characterized by scanning electron microscope (SEM, TESCAN MIRA 3, Czech Republic). The macroscopic appearance and structural colors of the PCs and PCHs were photographed with a digital camera (FDR-AX45, Sony, Japan) at an incident angle of 90°. The color information (such as hue values, RGB values) of the images was analyzed by Photoshop software (Adobe, CA, USA). The weight of hydrogels was recorded by an electric balance (ME204, Mettler-Toledo, Switzerland). The reflection spectra of the PCs were characterized by an UV–vis–near infrared spectrophotometer (Lambda 1050+, PerkinElmer, USA), and then normalized within Origin software (OriginLab, MA, USA). The mechanical properties of the PCHs were evaluated on a universal testing machine (UTM2503, Shenzhen Suns Technology, China) in tensile mode at a tensile speed of as 20 mm/min.

Test of glucose response

To test the glucose response, AA-AM-AFPBA hydrogels and the prepared PCHs (either single network or double network, either blue or green color) were immersed into glucose solutions with different concentrations of 0 mM, 6.6 mM, 13.2 mM, 19.8 mM, and 26.4 mM, respectively. After reaction for 15–30 min, the samples were removed from the solutions, and the volume and color changes were recorded by digital camera, and the weight was recorded with an electric balance. To test the reversible glucose response, AA-AM AFPBA hydrogels and PCHs were successively immersed into glucose solutions from low concentration (0 mM) to high concentration (26.4

mM), then successively immersed back into low glucose concentrations till 0 mM. After each reaction for 15–30 min, the volume changes, relative weight changes and color changes of the samples were recorded. The swelling ratio of the samples was calculated using following equation:

$$Swelling\ ratio\ (\%) = \frac{V_n}{V_0} \times\ 100\%$$

where V_0 and V_n represent the volume of hydrogels (in mm^3) after swelling in 0 mM and in concentrated glucose solution, respectively.

The relative weight of the samples was calculated using following equation:

$$Relative\ weight\ (\%) = \frac{M_n}{M_0} \times\ 100\%$$

where M_0 and M_n represent the weight of hydrogels (in gram) after swelling in 0 mM and in concentrated glucose solution, respectively.

Preparation of pH-responsive hydrogels

The pH-responsive hydrogels were prepared based on AM but without AA, since the later one is acidic and affect the pH response. Briefly, the prepolymer solution was prepared by dissolving the following ingredients in deionized water: 10% (w/v) AM, 5‰ (w/v) KPS, 1.5‰ (w/v) MBAA and 0.015‰ (w/v) PR for alkaline environment, or 10% (w/v) AM, 5‰ (w/v) KPS, 1.5‰ (w/v) MBAA and 0.015‰ (w/v) BB for acidic environment. The prepolymer solution was added dropwise into the mold, and heated at 60 °C on a heating table for 1 h for crosslinking. The obtained hydrogels incorporated with PR or BB were labelled as PAM-PR or PAM-BB, which were designed for response to alkaline or acidic environment, respectively.

Test of pH response

Alkaline-responsive PAM-PR hydrogels were immersed in alkaline solutions ranging of 7.0 ~ 9.0. Meanwhile, acidic-responsive PAM-BB hydrogels were immersed in acidic solution with pH 3.5 ~ 5.0. The color changes of hydrogels were recorded by digital camera accordingly. Subsequently, the changes of the hue values and RGB values of the images were analyzed by Photoshop software.

Preparation of temperature-responsive hydrogels

Temperature-responsive hydrogels were also prepared based on AM but not AA, since the later one disrupted the structure of thermochromic powders. Briefly, 20% (w/v) AM, 5‰ (w/v) KPS, 1.5‰ (w/v) MBAA, and 5‰ (w/v) blue or green thermochromic powders were dissolved in deionized water, to prepare a prepolymer solution. Here, both thermochromic powders have a critical temperature of 38 °C, where the blue thermochromic powders immediately change from blue to gray at 38 °C, whereas the green thermochromic powders immediately changed from gray to light green at 38 °C. Then the prepolymer solution was added dropwise into the mold, heated on a heating table at 60 °C for 1 h. The obtained hydrogels containing blue or green thermochromic powders was named as PAM-B and PAM-G, respectively.

Test of temperature response

The obtained PAM-B and PAM-G hydrogels were successively placed on a heating table at temperatures of 37 °C, 38 °C, 39 °C and 40 °C, and then placed back to 37 °C. The color changes of the hydrogels were recorded accordingly. Afterwards, the color information of the images was analyzed using Photoshop software.

Cell compatibility of PCHs

Cell compatibility of PCHs was evaluated using CCK-8 assay. First, PCHs were incubated in DMEM/F12 cell culture medium (Thermo Fisher Scientific) at a density of 0.1 g/mL at 37 °C for 24 h, then PCH extract was obtained after filtration. Human skin fibroblast (HSF) cells (Hunan Fenghui Biotechnology Co., Ltd, China) were seeded into 96-well plate at 5000 cells /well, and cultured in PCH extract with different concentration of 100%, 50%, 25% and 12.5%. Cells cultured in DMEM/F12 medium served as control. After cell culture for 24–48 h, 10 μL CCK-8 solution (Beyotime, China) was added into each well and incubated at 37 °C for 2 h. The absorbance at 450 nm of each well was measured by Microplate Readers (Thermo Fisher Scientific). And the relative cell viability was calculated by:

$$Cell\ viability = \frac{A_t}{A_c} \times\ 100\%$$

where A_t and A_c represent the absorbance of the test sample and the control group, respectively.

In vivo monitoring during diabetic wound healing

All animal experiments were performed with approval by the Institutional Animal Care and Use Committee of Wuhan University (IACUC, No. WP20230449). C57BL/6 mice (male, ~ 20 g) were raised in an SPF environment. Diabetic mice model was induced by intraperitoneal injection of streptozotocin (STZ, Sigma-Aldrich) at a dose of 100 mg/kg for three times according to our empirical experience [22, 39, 42]. The tail vein blood glucose levels were continuously monitored, and diabetic mouse model was successfully created when blood glucose surpassed 16.6 mM.

Afterwards, the dorsal of diabetic mice was shaved, and a round wound injury with a diameter of 6 mm was created on the dorsal of mice using a biopsy punch. Different hydrogels, including double network PCHs, PAM-PR and PAM-B were applied to cover the wound sites. The color changes of the hydrogels were photographed for image analysis, and different biomarker levels (including glucose, pH and temperature) were calculated according to the color information of the hydrogels as above described.

During diabetic wound healing, the wounds were covered with double network PCHs, DuoDerm® wound dressing (ConvaTec, UK) as a positive control, and left untreated as a negative control ($n=7$). The wounds were daily photographed during healing process, and the wound areas were measured by Image J software (NIH, USA).

Statistical analysis

For in vitro experiments, at least three repetitions were used for each group, and the experiments were replicated at least three times. For in vivo study, at least 5 mice were used for each group. Data were presented as mean ± standard deviation (SD). Statistical analysis was performed using Student's t-test for two groups by Origin software (OriginLab, MA, USA). Data were considered as statistically significant difference when P value of <0.05 versus the indicated groups, and as not significant when P value of >0.05.

Results and discussion

Preparation and characterization of silica PC structure

First, periodic PCs with different structural colors were prepared prior to the fabrication of functional PCHs. With an improved horizontal deposition method in our previous report [41], PC structures with different macroscopic structural colors from red to blue were obtained by fast self-assembly of silica nanoparticles with different sizes within 4 h (Fig. 2a). Specifically, the structural colors of the obtained PCs were modulated by the diffracted wavelength (λ) of the reflected light, which obeys Bragg equation:

$$n\lambda = 2d\sin\theta$$

where n is the diffraction number, d represents the minimum period of the structure, and θ is the angle between the incident light and the diffraction plane.

According to the Bragg equation, when the observation angle θ was fixed, the diffracted wavelength λ of the reflected light was only proportional to the period d. Therefore, the macroscopic structure colors of PCs can be regulated simply by changing the particle sizes of silica nanoparticles. When the diameter of silica nanoparticles varied from 320 nm, 300 nm, 260 nm, 250 nm to 240 nm, the macroscopic structural colors of the obtained PCs appeared from red, yellow, green, light blue to blue, respectively (Fig. 2a). Accordingly, the reflection spectra of the obtained PCs demonstrated the differences in the reflected lights (Fig. 2b). The peak wavelengths changed from 618 nm to 597 nm, 572 nm, 505 nm, 489 nm, and 451 nm (Fig. 2b), and the peak positions were in accordance with the Bragg equation.

Moreover, SEM images of the obtained PCs demonstrated that the self-assembled silica were closely packed into periodic structure (Fig. 2c_i), with a thickness of about 7 μm, which consisted of 10 layers of silica nanoparticles (Fig. 2c_{ii}). The periodic structure induced strong reflected lights, moreover, with the regulation of periodic parameters of silica nanoparticles, different structural colors of PCs were achieved (Fig. 2a-b). Additionally, SEM images also revealed the tightly arranged PC structure obtained from silica nanoparticles with different sizes (Fig. S1), which corresponded to different macroscopic structural colors of PCs (Fig. 2a).

Preparation and characterization of glucose-responsive hydrogels

Single network and double network PCHs were subsequently developed based on the above PC structure, by infiltration of glucose-responsive AA-AM-AFPBA hydrogels (Fig. 1a-b) into the interstitial space of the PCs (Fig. 1c) or into the inverse opal structure of PCs (Fig. 1d), respectively.

Briefly, acrylic acid (AA), acrylamide (AM) and glucose-responsive molecule of AFPBA [38–40], which has specific affinity to glucose [43], were copolymerized via radical polymerization as well as hydrogen bonding, to obtain glucose-responsive AA-AM-AFPBA hydrogels (Fig. 1a). Based on the reversible binding of phenylboronic acid of AFPBA molecule with the *cis*-diol group of glucose (Fig. 1b) [38, 39, 43], the obtained AA-AM-AFPBA hydrogel was able to exhibit reversible swelling changes according to different glucose levels in physiological range. In higher glucose concentration, more glucose competed with the boronated species to form cyclic boronate esters, resulting in larger swelling of AA-AM-AFPBA hydrogels (Fig. S2). The higher the glucose concentrations, the greater the swelling of the hydrogels (Fig. S2a), the swelling of AA-AM-AFPBA hydrogel increased from 100.8% ± 1.5%–205.4% ± 1.2% when the glucose solutions increased from 0 to 26.4 mM (Fig. S2b). Moreover, the glucose response behavior of AA-AM-AFPBA hydrogels was reversible. When the glucose concentrations decreased from 26.4 mM to 0 mM, the swelling of AA-AM-AFPBA hydrogels decreased from 205.4% ± 1.2%–101.4% ± 2.1%, almost returned to the original sizes (Fig. S2a). Meanwhile, the weight of AA-AM-AFPBA

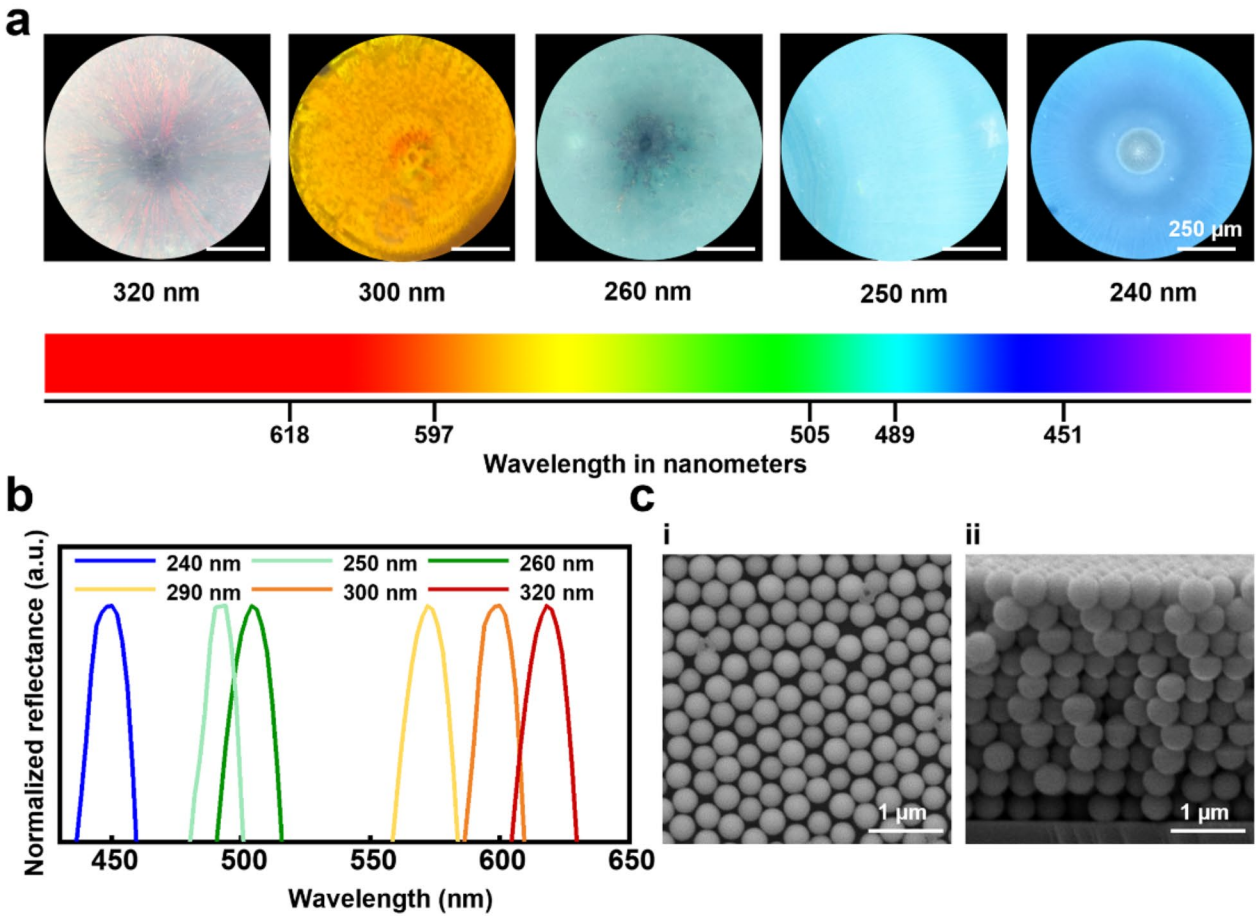

Fig. 2 Characterization of fast self-assembled photonic crystals (PCs). (**a**) Optical images of PCs obtained using silica nanoparticles with diameters of 320 nm, 300 nm, 260 nm, 250 nm and 240 nm, respectively. The bottom bar corresponds to the visible light spectrum with indicated wavelengths. (**b**) Normalized reflection spectra of PCs obtained with silica nanoparticles of diameters of 320 nm, 300 nm, 290 nm, 260 nm, 250 nm and 240 nm, respectively. (**c**) Representative SEM images of PCs in the front view (i) and in the side view (ii)

hydrogels changed accordingly (Fig. S2c). The higher the glucose concentration, the greater the weight of the hydrogels (Fig. S2c). The relative weight of the hydrogels increased from 100.8% ± 3.4%–205.4% ± 4.6% when the glucose solution increased from 0 mM to 26.4 mM (Fig. S2c), and the relative weight of the hydrogels decreased to 101.0% ± 3.4% when glucose concentration returned to 0 mM (Fig. S2c). Benefiting from the reversible glucose response, the integration of AA-AM-AFPBA hydrogels with PCs with intuitive structural colors therefore has good potentials for visual monitoring of glucose in the range of physiological levels.

Preparation and characterization of PCHs

Single network PCHs were developed with the infiltration of glucose-responsive AA-AM-AFPBA hydrogels into the interspace of silica PC structures under capillary force, followed by polymerization under 60 °C for 1 h (Fig. $1c_{i-ii}$). Further, the removal of silica nanoparticles by hydrofluoric acid (HF) etching resulted in an inverse opal structure of AA-AM-AFPBA hydrogels (Fig. $1c_{iii}$). Similarly, an inverse opal structure of non-glucose-responsive AA-AM hydrogels was prepared (Fig. $1d_{i-ii}$). Further, double network PCHs were prepared by the infiltration of glucose-responsive AA-AM-AFPBA hydrogels into the empty space of inverse opal structure of AA-AM hydrogels (Fig. $1d_{iii}$), followed by photopolymerization under UV irradiation for 3 min.

SEM images were used to characterize the preparation process of single network and double network PCHs. First, SEM images revealed the infiltration of AA-AM-AFPBA or AA-AM hydrogels into the gap of silica nanoparticles (Fig. 3a and c). After etching by HF, the silica nanoparticles disappeared, leading to respective hydrogels with in situ nanopores (Fig. 3b and d), which proved the inverse opal structure of AA-AM-AFPBA or

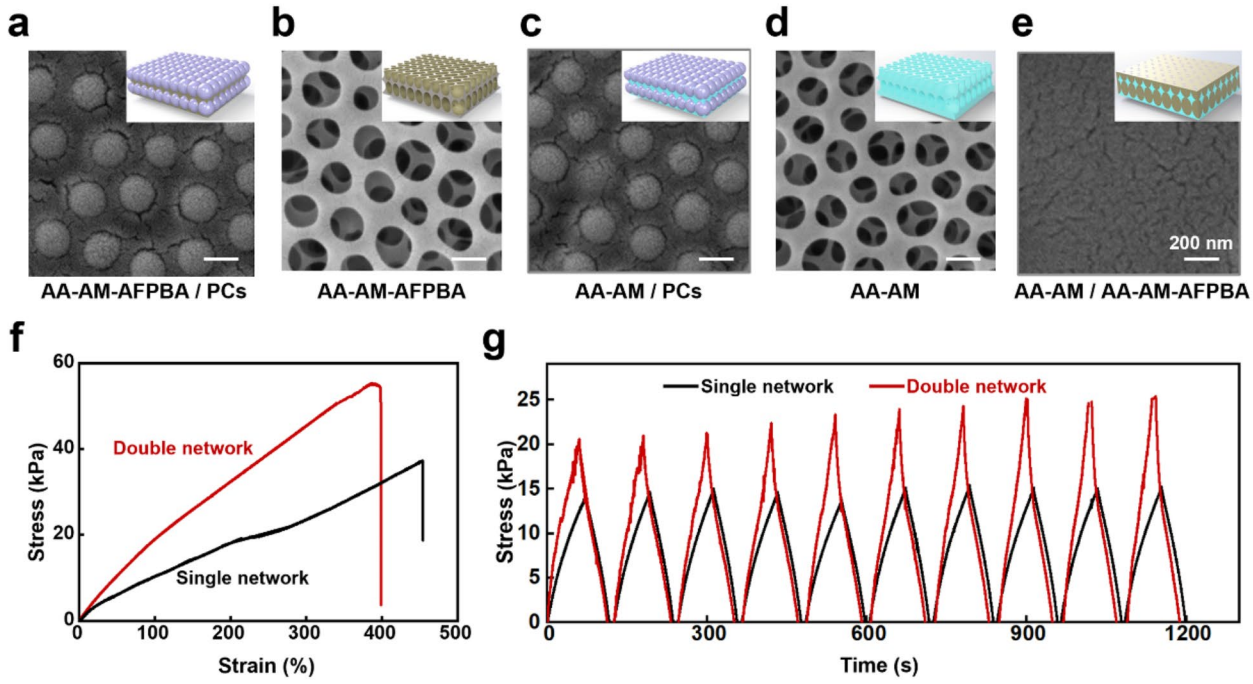

Fig. 3 Characterization of single network and double network PCHs. (**a**-**b**) SEM images during preparation of single network PCHs, including PCs infilled with AA-AM-AFPBA hydrogels (**a**), and inverse opal structure of AA-AM-AFPBA hydrogels (**b**). (**c**-**e**) SEM images during preparation of double network PCHs, including PCs infilled with AA-AM hydrogels (**c**), inverse opal structure of AA-AM hydrogels (**d**), and double network PCHs consisted of AA-AM and AA-AM-AFPBA hydrogels (**e**). (**f**) Tensile property of single network and double network PCHs. (**g**) Cyclic tensile properties of PCHs during 10 tensile cycles, the strain was set as 200%

AA-AM hydrogels, respectively. The opal structure and inverse opal structure of both hydrogels exhibited good periodic structure before and after etching (Fig. 3a-d). After secondary crosslinking (Fig. 1d$_{iii}$), SEM image showed a uniform morphology of the composite hydrogels (Fig. 3e), indicating the successful infiltration and binding of AA-AM-AFPBA into the inverse opal structure of AA-AM hydrogels.

The mechanical properties of the obtained single network and double network PCHs were characterized by tensile tests. The single network PCHs exhibited a tensile strength of 33.8 ± 0.6 kPa, with a maximum strain of 454.1% ± 0.9% (Fig. 3f). Compared to single network PCHs, double network PCHs showed an increased tensile strength to 53.6 ± 0.8 kPa, but with a slightly decreased elongation to 398.6% ± 1.4% (Fig. 3f). Further, the mechanical properties of the PCHs were evaluated by cyclic tensile tests. After 10 cycles of stretching with an elongation of 200%, both single network and double network PCHs retained a stable tensile property (Fig. 3g).

In double network PCHs, AA-AM-AFPBA and AA-AM skeleton themselves were crosslinked in the opal and inverse opal structure of PCs (Fig. 1d$_{iii}$), respectively, moreover, AA-AM-AFPBA and AA-AM were copolymerized at their interface via radical crosslinking and hydrogen bonding (Fig. 1d$_{iii}$) [39, 43], forming a bulk hydrogel network, which contributed to the increased tensile strength and slightly decreased elongation at break as compared to the porous structure of single network PCHs. Moreover, abundant hydrogen bonds existed in AA-AM and AA-AM-AFPBA skeletons, as well as at their interface (Fig. 1d$_{iii}$), which enhanced the cohesion of double network PCHs [44, 45], and the reorganization of hydrogen bonding and dynamic chain segment motion led to the enhanced mechanical strength of double network PCHs [46–48].

Overall, both single network and double network PCHs exhibited a tensile strength of greater than 30.0 kPa, and showed good elasticity and durability against external forces, which is beneficial for potential application as diabetic wound dressing.

Visual glucose monitoring of PCHs

Based on the above excellent structural colors and mechanical properties of the PCHs, the glucose responsive performance and visual readout of glucose by PCHs was investigated, since glucose monitoring is especially critical in diabetic wounds, which can reflect the blood glucose levels and serve as a prognostic indicator for diabetes [5]. For double network PCHs, the structural colors of PCHs became stable after 15 min upon reaction with glucose solutions (Fig. S3a). When the glucose

concentration increased from 0 to 26.4 mM, the structural color of blue PCHs gradually changed from blue to green (Fig. 4a), and the green PCHs gradually shifted from green to red colors (Fig. 4b), both PCHs exhibited a red shift in structural colors. In contrast, as the decrease of glucose concentrations from 26.4 mM to 0 mM, the structural color of blue PCHs gradually returned from green to blue (Fig. 4a), and the green PCH gradually returned from red to green (Fig. 4b), the structural color of both PCHs underwent a blue shift. When immersed in a higher concentration of glucose solutions, double network PCHs exhibited a larger swelling due to the

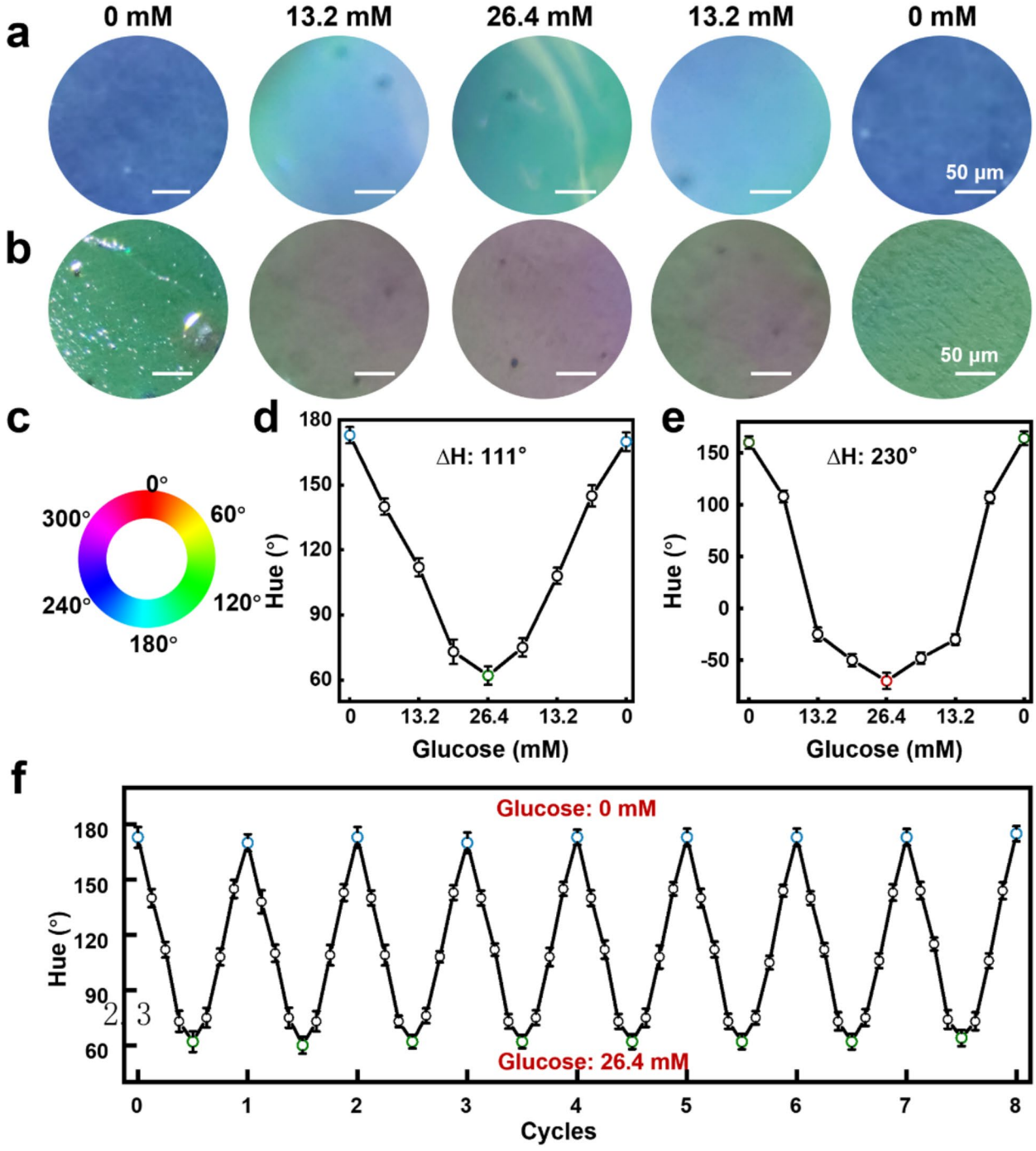

Fig. 4 Glucose response of double network PCHs. (**a**-**b**) Optical images of blue PCHs (**a**) and green PCHs (**b**) reacted with different glucose solutions from 0 to 13.2 mM, 26.4 mM, and back to 13.2 mM and 0 mM. (**c**) Hue circle with indicated hue values at corresponding positions. (**d**-**e**) Hue value changes of blue PCHs (**d**) and green PCHs (**e**) corresponding to changes in (**a**) and (**b**), respectively. (**f**) Hue value changes of blue PCHs during cyclic glucose response

glucose-responsive AA-AM-AFPBA motifs (Fig. S3b). According to Bragg equation, the increased distance in the diffraction planes therefore led to a redshift of the double network PCHs (Fig. 4a-b). In contrast, when immersed in a lower contraction of glucose solutions, the swelling of PCHs gradually decreased (Fig. S3a), the decrease in the diffraction planes resulted in a blueshift of the PCHs back to their original colors (Fig. 4a-b). The above result proved the good glucose sensitivity and reversibility of the double network PCHs.

Further, to better interpret the structural color changes of PCHs during glucose response, we used hue value of colors for characterization [36, 41]. Hue values were expressed from 0° to 360° on the color wheel, for example, 0°, 120° and 240° correspond to red, green and blue colors (Fig. 4c). With the increase of glucose concentration from 0 to 26.4 mM, the hue value of blue PCHs gradually changed from 173.0° ± 3.7° to 62.0° ± 4.2° (Fig. 4d), and the hue value of green PCHs varied from 160.0° ± 6.1° to -70° ± 5.6° (Fig. 4e). It is worth noting that the hue value changes for green PCHs (ΔH=230°) was larger than that of blue PCHs (ΔH=111°). When immersed the PCHs in glucose solutions ranging from 26.4 mM to 0 mM, the hue values of both blue and green PCHs gradually increased and returned to their original values (Fig. 4d-e), proving the reversible glucose response of double network PCHs. Based on the above results, we were able to achieve visual monitoring of glucose in physiological levels, according to the intuitive structural colors and the hue values of the double network PCHs (Fig. 4a-e).

Moreover, we investigated the cyclic glucose response of double network PCHs. Taking double network PCHs with blue structural color for an example, the PCHs exhibited cyclic changes between blue and green colors during the cyclic changes of glucose solutions, and the hue values of PCHs shifted between 172.0° ± 5.5 ° and 60.0° ± 4.5° (Fig. 4f), indicating a stable and repeatable response of double network PCHs during cyclic glucose changes. The reversible and stable glucose response with visual color transitions is important for application in wound-monitoring dressing.

Comparison of visual glucose monitoring of PCHs

We also investigated the glucose response and visual readout performance of single network PCHs in different glucose solutions. Similar to the double network PCHs, the single network PCHs also exhibited a visual glucose response upon different glucose concentrations (Fig. S4a-b), and this visual response was reversible (Fig. S4c-d) and stable during cyclic glucose changes (Fig. S4e). Compared to previous report, single network PCHs was prepared with 3-acrylamidophenylboronic acid (APBA) crosslinked with ethylene glycol dimethyl acrylate (EGDMA) [49], visual monitoring of glucose was achieved in a target ionic-strength solutions with pH>9 but not at pH≤7, with a detection range of glucose varied from 0 to 9 mM [49]. Here, visual glucose monitoring was realized in physiological pH conditions (pH ~ 7) and physiological range of glucose levels (0 ~ 26.4 mM) (Fig. 4, Fig. S4), making the PCHs more suitable for practical application.

For both single network and double network blue PCHs, the structural colors of both PCHs changed from blue color to green color during the glucose response (Fig. S3a, inserted images). After glucose reaction, the swelling ratio of double network PCHs was slightly higher than that of single network PCHs (Fig. S3b), but the changes of hue values of single network PCHs was slightly larger than that of double network PCHs (Fig. S3c). However, with naked eyes, it was difficult to distinguish their difference in structural colors at the start and at the end of glucose reaction (Fig. S3a, inserted images). With naked eye observation, their glucose response speed was different. The glucose response of single network PCHs was completed in about 30 min, whereas this response of double network PCHs was shortened into 15 min (Fig. S3a), with an increased speed of twice to the end of glucose reaction.

To interpret the difference of this phenomenon, we analyzed the relative volume of glucose-responsive motifs in both single network and double network PCHs. In the self-assembled, tightly arranged PC structures (Fig. 2c, Fig. S1), if silica nanoparticles were ideally arranged into simple cubic structure, body-centered cubic (BCC) structure or face-centered cubic (FCC) structure, the relative volume of silica nanoparticles was 52%, 68% and 74%, respectively (Table S1) [50]. Therefore, the relative volume of glucose-responsive motifs of AA-AM-AFPBA hydrogels in double network PCHs was in the range of 52% ~ 74% (Table S2). In contrast, the relative volume of glucose-responsive motifs of AA-AM-AFPBA hydrogels in single network PCHs ranged in 48% ~ 26% (Table S2). The higher volume fraction of AA-AM-AFPBA hydrogels in double network PCHs probably contributed to a faster glucose response compared to the single network PCHs (Fig. S3a). Therefore, double network PCHs were selected for next in vivo study in animals.

Preparation and characterization of pH-responsive hydrogels

Besides, we developed pH-responsive hydrogels and investigated their reaction activity upon different pH environments, since pH level is important biochemical marker involved in many physiological processes in the body, such as inflammation, infection, and wound remodeling [25]. Here, we developed alkaline-responsive hydrogels by polymerization of AM in which incorporated with an alkaline indicator of phenol red (PAM-PR)

at 60 °C for 1 h. After successive immersion into solutions with pH from 7.0 to 9.0, PAM-PR hydrogels exhibited visible pH-responsive color changes, and the colors rapidly changed from yellow (pH 7) to red (pH 9) (Fig. S5a), corresponding to hue value changing from 38.0° ± 0.8° to -5.0° ± 1.2° (Fig. S5b), and the color transition was completed in 5 ~ 15 s. When the pH value of solutions decreased from 9.0 to 7.0, PAM-PR hydrogels rapidly returned from red to yellow colors (Fig. S5a), accordingly, the hue values changed from −5.0° ± 1.2° back to 40.0° ± 1.4° (Fig. S5b). These results proved that PAM-PR hydrogels not only achieved immediate pH response, but also this response was reversible. Moreover, PAM-PR hydrogels showed good stability and repeatability of pH response during 5 cycles of pH variation from 7.0 to 9.0 (Fig. S5c).

Meanwhile, acidic-responsive hydrogels were prepared by polymerization of AM incorporated with an acidic indicator of bromophenol blue (PAM-BB). When PAM-BB hydrogels were successively immersed in acidic solutions with pH 3.5 and 5.0, the colors of PAM-BB hydrogels rapidly changed from yellow to dark blue within 5 ~ 15 s (Fig. S5d), corresponding to the hue values changing from 52.0° ± 0.6° to 228.0° ± 2.5° (Fig. S5e). When PAM-BB hydrogels were immersed back in solutions with pH from 5.0 to 3.5, PAM-BB hydrogels rapidly changed back from dark blue to yellow colors (Fig. S5d), corresponding to the hue values changing from 228.0° ± 2.5° to 54.0° ± 1.6° (Fig. S5e). Therefore, PAM-BB hydrogels realized reversible pH response in an acidic environment. Similarly, PAM-BB hydrogels also showed good stability of pH response over cyclic pH changes (Fig. S5f). Based on the above results, we can monitor and calculate the pH levels of diabetic wounds, due to the color changes or hue values of PAM-BB or PAM-PR hydrogels (Fig. S5).

Preparation and characterization of temperature-responsive hydrogels

We also developed temperature-responsive functional hydrogels and investigated their reaction upon different temperature, since body temperature is one of the key vital signs, and wound temperature plays a fundamental role in infection and healing process [51]. Temperature-responsive hydrogels were prepared using AM with incorporation of either blue or green thermochromic powders with a critical temperature of 38 °C, named as PAM-B and PAM-G, respectively.

PAM-B hydrogels exhibited blue color at room temperature up to 37 °C (Fig. S6a, Fig. S7a). The color of PAM-B hydrogels rapidly changed from blue to colorless within 15 s when the temperature reached 38 °C and above, and changed from colorless to blue when the temperature decreased to below 38 °C, which illustrated the reversible temperature response of PAM-B hydrogels. We then transformed the visual images into RGB (red, green, blue) for analysis. During color changes, the values of three RGB channels changed in a similar trend. However, the red channel showed the most significant change, therefore was used to characterize the color change during temperature response. The changes in RGB values also showed a stable temperature response of PAM-B hydrogels during cyclic temperature changes (Fig. S6b-c), which demonstrated the stability of PAM-B hydrogel responded to temperature.

PAM-G hydrogels with green thermochromic powders was colorless at room temperature up to 37 °C (Fig. S6d, Fig. S7b), and rapidly changed from colorless to light green within 15 s when reached the critical temperature of 38 °C, and further changed to green when the temperature further increased to 40 °C (Fig. S6d), with RGB values in red channel decreased from 167.0 ± 1.6 to 118.0 ± 1.3 (Fig. S6e). In contrast, when the temperature decreased from 40 °C to 37 °C, the color of the PAM-G hydrogel returned to colorless (Fig. S6d), with RGB values in red channel returned to 164.0 ± 2.5 (Fig. S6e). Meanwhile, PAM-G hydrogels also showed stable temperature response during cyclic temperature changes (Fig. S6f). The above results suggested the potentials of PAM-B and PAM-G hydrogels in terms of visual monitoring of temperature, due to their reversible and stable color changes in response to temperature.

To exclude the effects of temperature and pH on the glucose-responsive AA-AM-AFPBA hydrogels, AA-AM-AFPBA hydrogels were immersed in high-temperature (Fig. S8a), acidic (Fig. S8b), or alkaline (Fig. S8c) environments for reaction. Compared to the control of neutral environment at room temperature (25 °C), the volume of AA-AM-AFPBA hydrogels did not change significantly after 30 min immersion in high temperature, acidic or alkaline environments (Fig. S8), indicating that the responsiveness of AA-AM-AFPBA hydrogel was not affected by temperature and pH values.

Detection performance of multiple bioindicators

Based on the above results, different modules of hydrogels can be integrated together to achieve detection of multiple bioindicators at the same time.

First, four different hydrogels (PCHs, PAM-BB, PAM-PR and PAM-B) for respective detection of glucose, acidic, alkaline and high-temperature environments were bonded together using medical glue (Fig. S9a). In an environment of 0 mM glucose and pH 7.0 at room temperature (25 °C), PCHs showed blue structural color due to 0 mM glucose (Fig. S9a), PAM-B hydrogel was in blue color due to room temperature (Fig. S9a), PAM-BB and PAM-PR hydrogel showed light green and orange, respectively, due the neutral environment (Fig. S9a).

Similarly, three different hydrogels (PCHs, PAM-PR and PAM-B) were bonded together for respective detection of glucose, alkaline and high-temperature environments (Fig. S9b-c). In an environment of increased glucose concentration (26.4 mM) and elevated temperature (38 °C), PCHs switched to green structural color due to 26.4 mM glucose (Fig. S9b), and PAM-B hydrogel became colorless due to high temperature (38 °C) (Fig. S9b), meanwhile, the color of PAM-PR hydrogel remained orange due to unchanged neutral environment.

Further, keeping the same glucose levels (26.4 mM) and temperature (38 °C) of the environment, whereas the pH increased to 8.5 (Fig. 9b-c), the color of PAM-PR hydrogel shifted to red due to alkaline environment (Fig. S9c), and the colors of PCHs and PAM-B hydrogel were stable due to the unchanged glucose levels and temperature (Fig. S9c).

The above results proved the independent response of each hydrogel module (Fig. S9), where the glucose response of PCHs was not affected by pH changes and temperature change, the alkaline response of PAM-PR hydrogel was not influenced by temperature and glucose levels, whereas the temperature response of PAM-B hydrogel was not affected by pH change as well as glucose changes.

Cell compatibility of PCHs

Cell compatibility of PCHs were evaluated using CCK-8 assay with HSF cells. After incubation with different concentration of PCH hydrogel extracts, cell viability of all groups was higher than 85% after 24–48 h incubation (Fig. S10a-b). Even with incubation with 100% PCH hydrogel extract, the cell viability was still as high as 92.6 ± 8.9% and 88.0 ± 6.8% after 24 h and 48 h incubation, respectively (Fig. S10a-b). This result indicated good cell compatibility of PCHs.

In vivo monitoring performance of hydrogels on diabetic wounds

Further, the in vivo visual monitoring of different biomarkers by functional hydrogels were investigated using a full-thickness wound model in diabetic mice. Due to the small wound area on the dorsal of mice, it was difficult to place multiple hydrogel modules onto the wound site at the same time. Therefore, different modules of hydrogels were separately applied onto the diabetic wound sites (Fig. S11), for the visual monitoring of physiological biomarkers including glucose levels, pH values and temperature separately during diabetic wound healing process. These biomarkers from wounds were monitored by hydrogel dressing and calculated according to the above methods in vitro.

Double network PCHs were applied on the diabetic wounds and removed after 15 min for visualization. After application to the diabetic wounds at day 0, the color of the blue PCHs changed from blue to green (Fig. 5a), the color was red-shifted, indicating hyperglycemia condition at diabetic wounds (Fig. 5b). Similarly, when applied to the diabetic wounds at day 0, PAM-PR hydrogel immediately changed from yellow to red colors (Fig. 5c), indicating an alkaline environment in diabetic wounds at day 0 (Fig. 5d). Meanwhile, when applied to the diabetic wounds at day 0, PAM-B hydrogels rapidly changed from blue to colorless (Fig. 5e), indicating a temperature over 38 °C at the diabetic wounds (Fig. 5f). The results showed that all three functional hydrogels can achieve the detection of respective physiological indicators of glucose levels, pH levels and temperature at the created diabetic wounds.

Furthermore, the visual monitoring of different physiological biomarkers during diabetic wound healing process were recorded. During diabetic wound healing, glucose levels at diabetic wounds characterized by double network PCHs slightly decreased from 19.6 ± 0.1 mM to 19.0 ± 0.1 mM from 0 to 4 days post injury (Fig. 5b), the glucose levels measured by PCHs were consistent with the glucose levels measured from tail vein blood (Fig. 5b). For healthy body, normal blood glucose values range from 3.9 to 6.1 mM during fasting and up to 7.9 mM at 2 h after meal. For diabetic body, fasting blood glucose exceeds 7.0 mM and 2-hour post-meal blood glucose exceeds 11.1 mM. During diabetic healing process, the wound glucose levels detected by the PCHs varied from 19.0 ± 0.1 mM to 19.6 ± 0.1 mM (Fig. 5b), this result was in consistent with the diabetic mouse model with a criteria of blood glucose level 16 mM, proving hyperglycemia during wound healing process. Previously, optical zwitterionic poly-carboxybetaine (PCB) hydrogel dressing was developed for glucose monitoring [8], and the glucose concentration of diabetic wounds in mice stayed stable at approximately 3.8 mM [8], which was far away from blood glucose concentrations. Comparably, our PCH dressing gave a more accurate wound glucose levels, which were consistent with physiological blood glucose levels.

The pH values of wounds in both control and diabetic mice were also measured by PAM-PR during healing process. From day 0 to day 4, the pH of diabetic wounds monitored by PAM-PR was in the range of 8.60 ± 0.05 ~ 8.70 ± 0.04, whereas the wound pH in healthy mice measured by PAM-PR hydrogels was 8.70 ± 0.03 ~ 8.90 ± 0.04 (Fig. 5d). In general condition, the normal skin is weakly acidic with a pH about 4 ~ 6, which supports the natural barrier function to resist microbial invasion. However, diabetic wounds were usually alkaline at a pH above 8 [52, 53], which were vulnerable to bacterial infections. The application of PAM-PR hydrogels demonstrated an alkaline environment (pH from 8.6 ~ 8.7) at

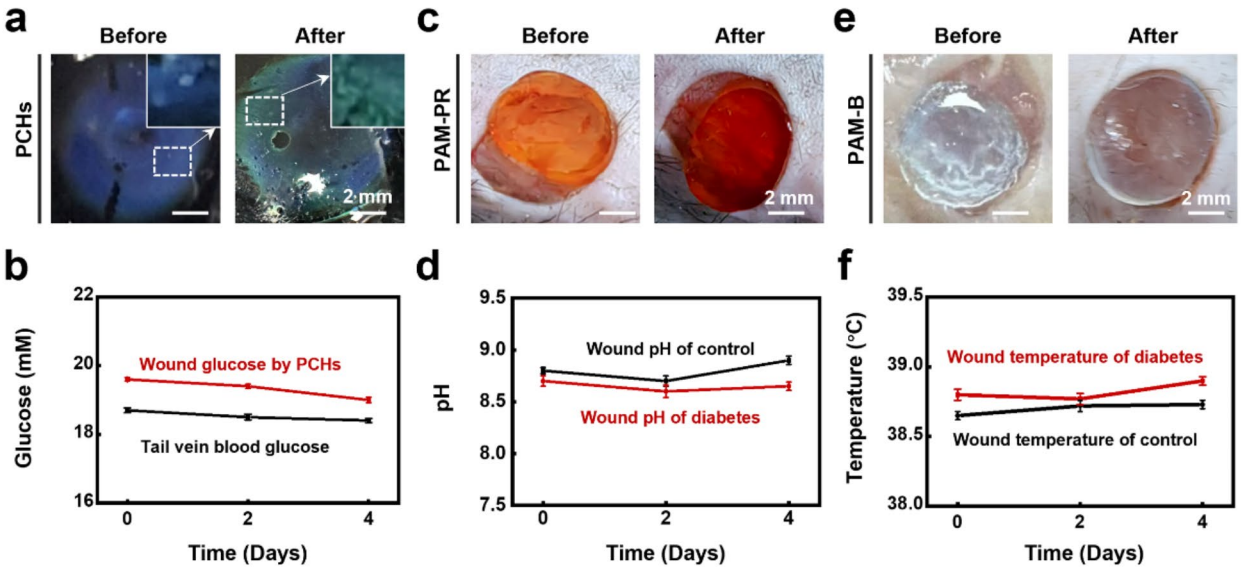

Fig. 5 In vivo monitoring of multiple biomarkers by functional hydrogels during diabetic wound healing. (**a**) Glucose response of double network PCHs before and after application to diabetic wound sites. (**b**) Glucose levels in diabetic wounds monitored by PCHs from 0 to 4 days post injury. Tail vein blood glucose levels was measured as control. (**c**) pH response of PAM-PR hydrogels before and after application to diabetic wounds. (**d**) Tracking of pH changes of diabetic wounds by PAM-PR hydrogels during healing. Health mouse wounds were used as control. (**e**) Temperature response of PAM-B hydrogel before and after application to diabetic wounds. (**f**) Monitoring of temperature changes of diabetic wounds by PAM-B hydrogel during healing. Health mouse wounds were used as control

diabetic wounds during early stage of healing (Fig. 5d). Our result was also in accordance with previous reported data, where wound pH measured by PCB significantly increased to alkaline (pH 7.5 ~ 9.0) at an early stage of diabetic wounds [8]. However, due to the gradually healed wound process, fewer and fewer wound exudate resulted in difficulty in further monitoring of wound pH by PAM-PR hydrogels during late stage of wound healing.

Meanwhile, the temperature of wounds in both control and diabetic mice were measured by PAM-B hydrogels during healing process. From 0 to 4 days post injury, the wound temperature of diabetic mice 38.70 ± 0.04 °C to 38.90 ± 0.03 °C, closed to the wound temperature of healthy mice varying from 38.60 ± 0.04 °C to 38.70 ± 0.03 °C (Fig. 5f). It's known body temperature in healthy individuals is ideally around 36 °C to 37 °C. However, diabetic wound temperature was widely variable depending on wound etiology and wound locations [54]. Previous studies reported an average wound temperature of 32.7 °C of diabetic foot ulcers in week 1 [51], whereas the surface temperature of an infected wound ranged from 38 °C to 42 °C [55]. Herein, PAM-B hydrogels can sensitively detect the high temperature (from 38.6 ~ 38.9 °C) at the early stage of healing, indicating an infection and inflammatory response presented in diabetic wounds.

We also monitored the diabetic wound healing process. Diabetic wounds in mice were covered with different dressing groups, including double network PCHs, commercialized DuoDerm® dressing as positive control, and left untreated as negative control. Both DuoDerm® dressing and control groups showed similar healing process in mice, and diabetic wounds were completely healed at day 15. At the early stage of healing from day 0 to day 6, wound healing in PCHs was slower compared to the control and DuoDerm® (Fig. S12a-b). From day 6 post injury, wound healing in PCHs accelerated, and the difference of wound areas among three groups became smaller (Fig. S12b). From day 8 to day 15, the wound areas of three groups further decreased, and showed similar wound areas (Fig. S12b). On day 15, the relative wound areas treated by control group, DuoDerm® and PCHs were 1.23 ± 0.08%, 0.85 ± 0.05% and 1.60 ± 0.10%, respectively (Fig. S12a), and no significant difference of wound areas was found among them (Fig. S12b), indicating the comparable healing activity of PCHs similar to DuoDerm® at the final stage of healing process. In addition, the body weight of diabetic mice slightly decreased without significant difference for different treatment groups (Fig. S12c), suggesting non-significant toxicity in vivo of PCHs comparable to the commercialized DuoDerm® dressing.

Conclusion

In conclusion, we developed a functional hydrogel system for in situ visual monitoring of multiple indicators of diabetic wounds, and successfully validated their ability for

visual monitoring of glucose levels, pH and temperature in vitro and in vivo in diabetic mice. For glucose monitoring, single network and double network PCHs was obtained based on PCs with intuitive structural colors and polymerization of acrylamide, acrylic acid and glucose-responsive AFPBA molecules. Both single network and double network PCHs exhibited good mechanical properties, and showed reversible and stable response to glucose solutions with visual color changes, where double network PCHs showed a twice faster glucose response than single network PCHs. The PCHs were successfully applied on the diabetic wounds in mice for quantitative feedback for in vivo glucose levels, and the wound glucose levels monitored by PCHs (19.0 ~ 19.6 mM) was comparable with tail vein blood glucose testing. Meanwhile, pH-responsive and temperature-responsive hydrogels were obtained from polymerization of acrylamide supplemented with acid-base indicators or thermochromic powders, respectively. PAM-PR hydrogels showed good pH response with sensitive color changes in vitro, and demonstrated an alkaline wound environment at diabetic wounds (pH 8.6 ~ 8.7). In addition, PAM-B hydrogels showed significant color changes when reached a critical temperature of 38 °C, and demonstrated an increased temperature (38.7 ~ 38.9 °C) in diabetic wounds. This multifunctional hydrogel system is important for intervention and indication of the physiological states of diabetic wounds with a convenient and direct visual readout with naked eyes, allowing for easier readout of the levels of wound indicators. This system provides an effective and visual monitoring during diabetic wound healing, and has potentials toward the development of the next generation of digitally visualized wound dressings. Moreover, the future integration of visual monitoring system with therapeutic delivery system is advantageous for both continuous monitoring and accelerated healing of diabetic wounds, and has great potential applications in wound care and wound management.

Supplementary Information

The online version contains supplementary material available at https://doi.org/10.1186/s12951-024-02905-7.

Supplementary Material 1

Acknowledgements
Not applicable.

Author contributions
Xuxia Yang: data curation, formal analysis, writing – original draft; Langjie Chai: data curation, formal analysis; Zhuo Huang: investigation and methodology; Bo Zhu: software; Haiyang Liu, Zhantian Shi and You Wu: investigation and methodology; Liang Guo and Longjian Xue: supervision; Yifeng Lei: conceptualization, funding acquisition, supervision, writing – review & editing. All authors reviewed the manuscript.

Funding
This work was supported by the National Natural Science Foundation of China (No. 82172096), Shenzhen Science and Technology Program (No. JCYJ20220530140610022), and Zhongnan Hospital Fund for Translational Medicine and Interdisciplinary Research (No. ZNJC202328).

Data availability
No datasets were generated or analysed during the current study.

Declarations

Ethics approval and consent to participate
All animal experiments were approved by the Institutional Animal Care and Use Committee of Wuhan University.

Consent for publication
All authors agree for publication.

Competing interests
The authors declare no competing interests.

Author details
[1]School of Power and Mechanical Engineering, The Institute of Technological Science, Wuhan University, Wuhan 430072, China
[2]Department of Plastic Surgery, Zhongnan Hospital of Wuhan University, Wuhan 430071, China
[3]Wuhan University Shenzhen Research Institute, Shenzhen 518057, China

Received: 9 July 2024 / Accepted: 3 October 2024
Published online: 12 October 2024

References

1. Daneman D. Type 1 diabetes. Lancet. 2006;367:847–58.
2. Falanga V. Wound healing and its impairment in the diabetic foot. Lancet. 2005;366:1736–43.
3. Armstrong DG, Boulton AJM, Bus SA. Diabetic foot ulcers and their recurrence. N Engl J Med. 2017;376:2367–75.
4. Li Y, Duan Y, Lin J, Liao J, Xu C, Xue F, Duan Y. Controlled synthesized of ternary Cu-Co-Ni-S sulfides nanoporous network structure on carbon fiber paper: a superior catalytic electrode for highly-sensitive glucose sensing. J Nanobiotechnol. 2024;22:377.
5. Xiang T, Guo Q, Jia L, Yin T, Huang W, Zhang X, Zhou S. Multifunctional hydrogels for the healing of diabetic wounds. Adv Healthc Mater. 2024;13:2301885.
6. Guo Z, Liu H, Dai W, Lei Y. Responsive principles and applications of smart materials in biosensing. Smart Mater Med. 2020;1:54–65.
7. Mirani B, Hadisi Z, Pagan E, Dabiri SMH, van Rijt A, Almutairi L, Noshadi I, Armstrong DG, Akbari M. Smart dual-sensor wound dressing for monitoring cutaneous wounds. Adv Healthc Mater. 2023;12:2203233.
8. Zhu Y, Zhang J, Song J, Yang J, Du Z, Zhao W, Guo H, Wen C, Li Q, Sui X, Zhang L. A multifunctional pro-healing zwitterionic hydrogel for simultaneous optical monitoring of pH and glucose in diabetic wound treatment. Adv Funct Mater. 2019;30:1905493.
9. Guo H, Bai M, Zhu Y, Liu X, Tian S, Long Y, Ma Y, Wen C, Li Q, Yang J, Zhang L. Pro-healing zwitterionic skin sensor enables multi-indicator distinction and continuous real-time monitoring. Adv Funct Mater. 2021;31:2106406.
10. Mai H, Wang Y, Li S, Jia R, Li S, Peng Q, Xie Y, Hu X, Wu S. A pH-sensitive near-infrared fluorescent probe with alkaline pKa for chronic wound monitoring in diabetic mice. Chem Commun. 2019;55:7374–7.
11. Zong Y, Zong B, Zha R, Zhang Y, Li X, Wang Y, Fang H, Wong W-L, Li C. An antibacterial and anti-oxidative hydrogel dressing for promoting diabetic wound healing and real-time monitoring wound pH conditions with a NIR fluorescent imaging system. Adv Healthc Mater. 2023;12:2300431.
12. Xu Z, Fan J, Tian W, Ji X, Cui Y, Nan Q, Sun F, Zhang J. Cellulose-based pH-responsive Janus dressing with unidirectional moisture drainage for exudate management and diabetic wounds healing. Adv Funct Mater. 2024;34:2307449.
13. Xiao J, Zhou Z, Zhong G, Xu T, Zhang X. Self-sterilizing microneedle sensing patches for machine learning-enabled wound pH visual monitoring. Adv Funct Mater. 2024;34:2315067.

14. Huang J, Zheng Y, Niu H, Huang J, Zhang X, Chen J, Ma B, Wu C, Cao Y, Zhu Y. A multifunctional hydrogel for simultaneous visible H_2O_2 monitoring and accelerating diabetic wound healing. Adv Healthc Mater. 2024;13:2302328.
15. Garland NT, Song JW, Ma T, Kim YJ, Vázquez-Guardado A, Hashkavayi AB, Ganeshan SK, Sharma N, Ryu H, Lee M-K, et al. A miniaturized, battery-free, wireless wound monitor that predicts wound closure rate early. Adv Healthc Mater. 2023;12:2301280.
16. Hwang J, Seo Y, Jeong D, Ning X, Wiraja C, Yang L, Tan CT, Lee J, Kim Y, Kim JW, et al. Monitoring wound healing with topically applied optical nanoflare mRNA nanosensors. Adv Sci. 2022;9:2104835.
17. Singh K, Agarwal T, Kumar U, Pal S, Runthala A, Pan T-M, Wu CC. Optical biosensors for diabetes management: advancing into stimuli-responsive sensing mechanisms. Smart Mater Med. 2023;4:91–101.
18. Yetisen AK, Montelongo Y, da Cruz Vasconcellos F, Martinez-Hurtado JL, Neupane S, Butt H, Qasim MM, Blyth J, Burling K, Carmody JB, et al. Reusable, robust, and accurate laser-generated photonic nanosensor. Nano Lett. 2014;14:3587–93.
19. Elsherif M, Hassan MU, Yetisen AK, Butt H. Wearable contact lens biosensors for continuous glucose monitoring using smartphones. ACS Nano. 2018;12:5452–62.
20. Yetisen AK, Jiang N, Fallahi A, Montelongo Y, Ruiz-Esparza GU, Tamayol A, Zhang YS, Mahmood I, Yang S-A, Kim KS, et al. Glucose-sensitive hydrogel optical fibers functionalized with phenylboronic acid. Adv Mater. 2017;29:1606380.
21. Elsherif M, Hassan MU, Yetisen AK, Butt H. Glucose sensing with phenylboronic acid functionalized hydrogel-based optical diffusers. ACS Nano. 2018;12:2283–91.
22. Wu M, Zhang Y, Liu Q, Huang H, Wang X, Shi Z, Li Y, Liu S, Xue L, Lei Y. A smart hydrogel system for visual detection of glucose. Biosens Bioelectron. 2019;142:111547.
23. Wei M, Li X, Serpe MJ. Stimuli-responsive microgel-based surface plasmon resonance transducer for glucose detection using a competitive assay with concanavalin A. ACS Appl Polym Mater. 2019;1:519–25.
24. Zhang S, Wang L, Xu T, Zhang X. Luminescent MOF-based nanofibers with visual monitoring and antibacterial properties for diabetic wound healing. ACS Appl Mater Interfaces. 2023;15:9110–9.
25. Min Y, Han R, Li G, Wang X, Chen S, Xie M, Zhao Z. The pH-sensitive optical fiber integrated CMCS-PA@Fe hydrogels for photothermal therapy and real-time monitoring of infected wounds. Adv Funct Mater. 2023;33:2212803.
26. Zhang M, Qing G, Xiong C, Cui R, Pang D-W, Sun T. Dual-responsive gold nanoparticles for colorimetric recognition and testing of carbohydrates with a dispersion-dominated chromogenic process. Adv Mater. 2013;25:749–54.
27. Dey GR, Saha A. Surface engineered PLGA nanoparticle for threshold responsive glucose monitoring and self-programmed insulin delivery. ACS Biomater Sci Eng. 2021;7:4645–58.
28. Hou J, Li M, Song Y. Patterned colloidal photonic crystals. Angew Chem Int Ed. 2018;57:2544–53.
29. Cai Z, Li Z, Ravaine S, He M, Song Y, Yin Y, Zheng H, Teng J, Zhang A. From colloidal particles to photonic crystals: advances in self-assembly and their emerging applications. Chem Soc Rev. 2021;50:5898–951.
30. Ito MM, Gibbons AH, Qin D, Yamamoto D, Jiang H, Yamaguchi D, Tanaka K, Sivaniah E. Structural colour using organized microfibrillation in glassy polymer films. Nature. 2019;570:363–7.
31. Wang YL, Cui HQ, Zhao QL, Du XM. Chameleon-inspired structural-color actuators. Matter. 2019;1:626–38.
32. Fu FF, Shang LR, Chen ZY, Yu YR, Zhao YJ. Bioinspired living structural color hydrogels. Sci Rob. 2018;3:eaar8580.
33. Konopsky V, Mitko T, Aldarov K, Alieva E, Basmanov D, Moskalets A, Matveeva A, Morozova O, Klinov D. Photonic crystal surface mode imaging for multiplexed and high-throughput label-free biosensing. Biosens Bioelectron. 2020;168:112575.
34. Zhou Q, Dong K, Wei M, He B, Gao B. Rolling stone gathers moss: rolling microneedles generate meta microfluidic microneedles (MMM). Adv Funct Mater. 2024;34:2316565.
35. Lu M, Zhang X, Xu D, Li N, Zhao Y. Encoded structural color microneedle patches for multiple screening of wound small molecules. Adv Mater. 2023;35:2211330.
36. Zeng Y, Wang J, Wang Z, Chen G, Yu J, Li S, Li Q, Li H, Wen D, Gu Z, Gu Z. Colloidal crystal microneedle patch for glucose monitoring. Nano Today. 2020;35:100984.
37. Wang H, Liu Y, Chen Z, Sun L, Zhao Y. Anisotropic structural color particles from colloidal phase separation. Sci Adv. 2020;6:eaay1438.
38. Ma Y, He P, Xie W, Zhang Q, Yin W, Pan J, Wang M, Zhao X, Pan G. Dynamic colloidal photonic crystal hydrogels with self-recovery and injectability. Research. 2021; 2021:9565402.
39. Guo Z, Liu H, Shi Z, Lin L, Li Y, Wang M, Pan G, Lei Y, Xue L. Responsive hydrogel-based microneedle dressing for diabetic wound healing. J Mater Chem B. 2022;10:3501–11.
40. Huang Z, Wang M, Chai L, Chen H, Chen D, Li Y, Liu H, Wu Y, Yang X, He L, et al. Glucose-responsive, self-healing, wet adhesive and multi-biofunctional hydrogels for diabetic wound healing. Mater Today Bio. 2024;27:101159.
41. Liu H, Wang Y, Shi Z, Tan D, Yang X, Xiong L, Li G, Lei Y, Xue L. Fast self-assembly of photonic crystal hydrogel for wearable strain and temperature sensor. Small Methods. 2022;6:2200461.
42. Zhang Y, Wu M, Dai W, Chen M, Guo Z, Wang X, Tan D, Shi K, Xue L, Liu S, Lei Y. High drug-loading gold nanoclusters for responsive glucose control in type 1 diabetes. J Nanobiotechnol. 2019;17:74.
43. Liu L, Tian X, Ma Y, Duan Y, Zhao X, Pan G. A versatile dynamic mussel-inspired biointerface: from specific cell behavior modulation to selective cell isolation. Angew Chem Int Ed. 2018;57:7878–82.
44. Zheng K, Tong Y, Zhang S, He R, Xiao L, Iqbal Z, Zhang Y, Gao J, Zhang L, Jiang L, Li Y. Flexible bicolorimetric polyacrylamide/chitosan hydrogels for smart real-time monitoring and promotion of wound healing. Adv Funct Mater. 2021;31:2102599.
45. Wang L, Duan L, Liu G, Sun J, Shahbazi MA, Kundu SC, Reis RL, Xiao B, Yang X. Bioinspired polyacrylic acid-based dressing: wet adhesive, self-healing, and multi-biofunctional coacervate hydrogel accelerates wound healing. Adv Sci. 2023;10:2207352.
46. Wang Y, Huang X, Zhang X. Ultrarobust, tough and highly stretchable self-healing materials based on cartilage-inspired noncovalent assembly nanostructure. Nat Commun. 2021;12:1291.
47. Li X, Gong JP. Design principles for strong and tough hydrogels. Nat Rev Mater. 2024;9:380–98.
48. Li X, Cui K, Zheng Y, Ye YN, Yu C, Yang W, Nakajima T, Gong JP. Role of hierarchy structure on the mechanical adaptation of self-healing hydrogels under cyclic stretching. Sci Adv. 2023;9:eadj6856.
49. Feng X, Xu J, Liu Y, Zhao W. Visual sensors of an inverse opal hydrogel for the colorimetric detection of glucose. J Mater Chem B. 2019;7:3576–81.
50. Stachurski ZH. On structure and properties of amorphous materials. Materials. 2011;4:1564–98.
51. Derwin R, Patton D, Strapp H, Moore Z. The effect of inflammation management on pH, temperature, and bacterial burden. Int Wound J. 2023;20:1118–29.
52. Panzarasa G, Osypova A, Toncelli C, Buhmann MT, Rottmar M, Ren Q, Maniura-Weber K, Rossi RM, Boesel LF. The pyranine-benzalkonium ion pair: a promising fluorescent system for the ratiometric detection of wound pH. Sens Actuat B. 2017;249:156–60.
53. Zhu Z, Wang L, Peng Y, Chu X, Zhou L, Jin Y, Guo H, Gao Q, Yang J, Wang X, et al. Continuous self-oxygenated double-layered hydrogel under natural light for real-time infection monitoring, enhanced photodynamic therapy, and hypoxia relief in refractory diabetic wounds healing. Adv Funct Mater. 2022;32:2201875.
54. Gethin G, O'Connor GM, Abedin J, Newell J, Flynn L, Watterson D, O'Loughlin A. Monitoring of pH and temperature of neuropathic diabetic and nondiabetic foot ulcers for 12 weeks: an observational study. Wound Repair Regen. 2018;26:251–6.
55. Pang Q, Lou D, Li S, Wang G, Qiao B, Dong S, Ma L, Gao C, Wu Z. Smart flexible electronics-integrated wound dressing for real-time monitoring and on-demand treatment of infected wounds. Adv Sci. 2020;7:1902673.

Publisher's note